

Cite this: *Mater. Adv.*, 2022,  
3, 1115

# *Sapindus mukorossi* seed shell extract mediated green synthesis of CuO nanostructures: an efficient catalyst for C–N bond-forming reactions†

Tulan Chandra Saikia,<sup>a</sup> Saddam Iraqui,<sup>a</sup> Aslam Khan<sup>b</sup> and Md. Harunar Rashid<sup>ib\*</sup>

Catalytic reactions have been used for the synthesis of vital structures containing a C–N bond. The C–N bond-forming reaction is regarded as one of the most popular and efficient methods for the synthesis of many bioactive molecules. The design and application of environmentally friendly catalysts to reduce the amount of toxic waste is essential for such C–N bond-formation reactions. Herein, an effective biogenic approach is reported for the synthesis of size-tunable CuO nanostructures for use as catalysts in C–N bond-formation reactions. The synthesis has been carried out *via* a hydrothermal method in the presence of the seed shell extract of the *Sapindus mukorossi* plant followed by calcination in air. An X-ray diffraction (XRD) study reveals that the synthesized CuO nanostructures are crystalline and are free from any impurities. An electron microscopy study reveals that the shape of the CuO nanostructures is more or less homogeneous and that the phytochemicals present in the shell extract perform a key role in controlling the size of the formed CuO nanostructures. These newly developed CuO nanostructures can be used as efficient catalysts for the conjugate addition of amines to acrylonitrile with excellent yields under mild reaction conditions. The protocol is simple and applies to different substituted aryl and alkylamines. The catalyst system is more effective than other supported catalysts and needs no acid, base or ligand to promote the reaction. The catalyst is stable and is reusable up to five cycles with minimal loss of catalytic activity.

Received 6th October 2021,  
Accepted 24th November 2021

DOI: 10.1039/d1ma00927c

rsc.li/materials-advances

## 1. Introduction

For the last couple of decades, cupric oxide (CuO) nanoparticles (NPs) have gained substantial attention from a diverse field of academic and industrial researchers due to their versatility of application. CuO possesses a monoclinic structure with a narrow bandgap of 1.7 eV and is associated with attractive features like high stability, superior thermal conductivity, high chemical potential, photovoltaic properties and antimicrobial properties.<sup>1–5</sup> Because of these attractive physicochemical properties, CuO NPs deserve to be extensively studied for use in more efficient ways in diverse fields of technology such as in gas sensors, energy-storage systems, solar cells, biomedicine, catalysis, photocatalysis, high-temperature superconductors, supercapacitors, and so on.<sup>5–14</sup> Furthermore, due to their high

chemical potential, enhanced active surface area, chemical stability in a broad range of chemicals, and insolubility of CuO NPs in most solvents, they can act as an efficient heterogeneous catalyst in many important chemical conversions.<sup>7–9,15,16</sup> However, the physicochemical properties and application of CuO NPs are dependent on the size, shape, morphology, crystal patterns and accessible surface area of the constituent particles, which in turn largely depend upon the synthetic approach.<sup>13,17,18</sup> As a result, many physical and chemical methods, such as vapour deposition, arc discharge, sol-gel preparation, co-precipitation, hydrothermal, solvothermal and sonochemical methods, *etc.*, have been reported for the synthesis of CuO NPs.<sup>11–14,19,20</sup> Due to the use of expensive instrumentation or toxic chemicals as additives and/or solvents in most of the above-mentioned methods, they are neither environmentally benign nor cost-effective.<sup>21–23</sup> As a result scientists have gradually been adopting a bio-based process where either bioactive molecules or microorganisms such as algae, bacteria, fungi, *etc.*, are used as the stabilizing agent.<sup>23–25</sup> However, there are some limitations on the use of microorganisms, such as the toxicity of bacteria, and tedious isolation and incubation processes.<sup>21–23</sup> Hence, plant

<sup>a</sup> Department of Chemistry, Rajiv Gandhi University, Rono Hills, Doimukh 791 112, Arunachal Pradesh, India. E-mail: harunar.rashid@rgu.ac.in<sup>b</sup> King Abdullah Institute for Nanotechnology, King Saud University, Riyadh 11451, Saudi Arabia

† Electronic supplementary information (ESI) available. See DOI: 10.1039/d1ma00927c



extracts have been chosen in recent times as an ideal source of biomolecules for the synthesis of CuO NPs as it is easy and simple, safe, requires a low energy consumption and provides better stability of the formed NPs.<sup>21–23</sup> The plant extracts contain different types of bioactive molecules, which often act as a reducing agent, capping agent or stabilizing agent for various nanoparticle systems.<sup>21–23,26</sup> In the synthesis of CuO NPs, the phytochemicals mostly reduce the copper ions and then convert them into CuO.<sup>23,27,28</sup> Hence, a biogenic process that involves phytochemicals in the form of plant extracts has been proved to be a good alternative for the synthesis of CuO NPs. Considering the environmental hazards of most of the synthesis approaches, a handful of reports have been published in recent years using plant extracts either as additives or as reducing agents for copper ions.<sup>4,9,10,28–30</sup> It has been documented that the phytochemicals present in a particular plant extract at different concentrations provide a unique morphology, size and shape to the formed NPs.<sup>22,26,30</sup> Also, the type of plant extract, concentration, pH of the medium, time and temperature affect the reaction rate and hence the growth of CuO NPs.<sup>23,30</sup> Therefore, it is crucial to optimise a plant extract mediated synthesis method that may lead to the production of unique and highly functional CuO NPs. Motivated by recent reports, this study aims to use the aqueous seed shell extract of *Sapindus mukorossi* to synthesize CuO NPs for use as catalysts in organic reactions.

*Sapindus mukorossi* is well-known as the soapnut and is a member of the family Sapindaceae. It is commonly known as 'reetha', which has detergent, anti-inflammatory, antimicrobial, insecticidal, and other properties due to the presence of saponins and different bioactive molecules.<sup>31–34</sup> It is also a popular ingredient of ayurvedic preparations such as shampoos, cleansers and medicines for the treatment of eczema, psoriasis and for removing lice from the scalp.<sup>33,35</sup> The species is widely grown in the upper reaches of the Indo-Gangetic plains, Shivalik's and sub-Himalayan tracts at altitudes from 200 to 1500 m. The plant is also readily grown in the northeastern region of India. However, the particular tree commonly called the soapnut finds no value in the locality and is assumed to be a weed. Also, the economic value of the plant is very low in this area. In recent times, the water extract of different parts of the *Sapindus mukorossi* plant, which contains mainly saponins, flavonoids, carbohydrates, glycosides, tannins, proteins and amino acids, has been used as a reducing-cum-stabilizing agent for different metal nanomaterial systems.<sup>32,33,36–39</sup> However, the use of the extract of this particular plant for the synthesis of metal oxide is very limited. Jassal *et al.* reported the use of the aqueous extract of the fruit of *Sapindus mukorossi* for the synthesis of manganese oxide NPs.<sup>40</sup> In the present study, we intend to use the seed shell extract of *Sapindus mukorossi* to see if any improvement in the properties of CuO NPs can be made in terms of their morphology and applications. The additional advantage associated with this particular plant is that most of the time either medicinal or edible plants are used for the synthesis of nanomaterials, whereas the *Sapindus mukorossi* fruit – commonly called the soapnut – is not used for such applications nowadays.

Therefore, the successful utilization of the seed extract for controlling the nanoparticle growth could provide the weed with a market value in the near future and add value to sustainable development.

The conjugate addition of an –NH nucleophile to an  $\alpha,\beta$  unsaturated electrophile is the well-known aza-Michael addition for C–N bond formation. The products of the aza-Michael reaction are important building blocks of many bioactive molecules and pharmaceutical ingredients.<sup>41,42</sup> Long ago, the aza-Michael reaction was carried out in the presence of strong acids and bases with the formation of additional side products.<sup>43,44</sup> To improve and modify the aza-Michael reaction, different Lewis acids have been reported so far.<sup>45–47</sup> In addition, transition metal salts have also found application as catalysts for the aza-Michael reaction.<sup>48,49</sup> The important drawbacks of using such Lewis acids and transition metal salts are their lack of reusability, the formation of by-products and the threat of the incorporation of metal ions in the biologically important organic products during catalysis. Therefore, it is desirable to modify all of these chemical processes in a plausible, greener way that can add value to the already existing reaction procedures. One of the feasible and effective alternatives to these existing materials is heterogeneous catalysts. In industry, chemical reactions using heterogeneous catalysts has found greater importance over homogeneous catalysts due to the easy separation of a heterogeneous catalyst from the reaction medium and its possible reusability and green nature.<sup>50,51</sup> In the aza-Michael reaction, many heterogeneous catalysts, such as silica-supported  $\text{AlCl}_3$ ,<sup>52</sup> graphene oxide,<sup>53</sup> starch-supported pyridinium-based organo-catalysts,<sup>54</sup> phen-MCM-Br<sub>2</sub>,<sup>55</sup> kaolinite clays,<sup>56</sup> *etc.*, have been reported. However, many of them do not fit to the principles of Green Chemistry, such as atom economy, environmentally friendliness, expenses of synthesis, and the additional threat of the contamination of heavy metals in pharmaceutically oriented products. Therefore, it is necessary to look forward to a reaction pathway for the aza-Michael reaction using earth-abundant and inexpensive metal-based catalysts. CuO is one such earth-abundant and inexpensive metal oxide, which, due to its nano dimensions, has gained more importance as a heterogeneous catalyst in many organic reactions in recent times.<sup>7,8,15,16,57–59</sup> The size and shape of CuO NPs can greatly influence the catalytic activity of CuO NPs.<sup>60</sup> In view of the recent progress made in the use of plant extract-based CuO NPs in catalysis, the objective of this study is to use CuO NPs synthesized using the *Sapindus mukorossi* plant extract as an efficient catalyst in C–N bond-forming reactions between aryl amines and acrylonitrile in a greener way under ambient conditions.

## 2. Experimental section

### 2.1 Materials and methods

Copper(II) nitrate trihydrate, sodium hydroxide, methanol (EMPARTA), and aniline were purchased from Merck, India.



Acrylonitrile and the other substrates were purchased from Sigma-Aldrich and were used without any purification. The seeds of *Sapindus mukorossi* were collected from Gohain village in the Lakhimpur district of Assam, India. The required glassware was cleaned using freshly prepared *aqua-regia* solution (HCl:HNO<sub>3</sub> = 3:1, V/V), followed by washing with detergent and subsequent rinsing with double distilled water before being dried in an oven. All stock solutions were prepared using double-distilled water.

## 2.2 Isolation of flower extract

The collected seeds were cleaned by washing in tap water before being allowed to dry under sunlight. The shells of the dried seeds were separated using a knife and then the shells were crushed into powder form using a blender. The phytochemicals present in this powdered material (50 g) were extracted using Soxhlet apparatus with methanol as the extracting solvent (500 mL) at 60 °C for 6 h. After completion of this extraction process, the solvent was evaporated using a rotary evaporator to obtain a highly viscous mass, which was dried in a vacuum oven at 60 °C for 24 h. The dried mass (16 g, 32 wt%) was then kept in a refrigerator for further use. For synthesis of the CuO nanostructures, an aqueous solution of the dried extract (1.4 g; 10 mL) was prepared and filtered through cotton to remove any suspended solids.

## 2.3 Synthesis of CuO nanostructures

Synthesis of the CuO nanostructures was carried out *via* a hydrothermal method using the phytochemicals present in the seed shell extract of the *Sapindus mukorossi* plant as additive followed by calcination. Typically, an aqueous solution of the shell extract (14.0 wt%; 10 mL) was transferred into a 250 mL round bottom flask, fitted with a condenser, containing 88.0 mL of distilled water at 60 °C under stirring. To this extract solution was added 7.0 mL of 1.0 M copper nitrate solution, and the solution was mixed well under constant stirring at 60 °C. An aqueous solution of freshly prepared sodium hydroxide solution (35.0 mL; 1.0 M) was then added dropwise to this reaction mixture to raise the pH, and the stirring was continued for 30 min at the same temperature. The whole reaction mixture was then transferred into an autoclave (150 mL) and placed inside an air oven at 180 °C for 2 h. The transparent solution in the upper portion was discarded and the remaining suspension containing the black precipitate was centrifuged at 7000 rpm (REMI CPR 24 plus) for 15 min. The isolated solid was dispersed in water using ultrasonic vibration and the solid was collected by centrifugation. The process of dispersing the solid in water and centrifugation was repeated three times to purify the formed product. Finally, the isolated product was dried in a vacuum oven at 60 °C for 18 h. The dried sample was calcined at 500 °C for 4 h using a muffle furnace and the obtained product was labelled as CuO-1. A similar set of reactions was carried out by varying the extract concentration, keeping all other reaction conditions identical, and the samples were labelled as CuO-2 and CuO-3 (Table 1). Keeping all other conditions the same as above, another sample (CuO-4) was

Table 1 Reaction recipes for the synthesis of CuO nanoparticles

Components	CuO-1	CuO-2	CuO-3	CuO-4
Seed shell extract (wt%)	1.0	0.5	0.25	0
Copper(II) nitrate (M)	0.05	0.05	0.05	0.05
NaOH (M)	0.25	0.25	0.25	0.25

also prepared but without using any extract. All the synthesized CuO nanomaterials were characterized using different spectroscopic, microscopic and diffractometric techniques. The details of the characterization techniques used are provided in the ESI.†

## 2.4 C–N coupling reaction between amines and acrylonitrile

A mixture of amine (1.0 mmol), ethanol–water mixture (1.0 mL; 1:1 volume ratio), CuO NPs (2.0 mg) and acrylonitrile (2.5 mmol) was taken in a 25 mL round bottom flask fitted with a condenser and placed on a magnetic stirrer-cum-hotplate. The reaction mixture was then allowed to stir at 45 °C. The progress of the reaction was monitored using thin-layer chromatography (TLC). After completion of the reaction, 20.0 mL ethyl acetate was poured into the flask and the organic components were separated from the mixture by washing in a separating funnel with brine solution. The collected organic part was dried by filtration through anhydrous sodium sulphate. The pure product was extracted from the crude product using column chromatography (hexane/ethyl acetate = 10:1) using silica 100–200 mesh. The pure products were characterized using <sup>1</sup>H NMR and <sup>13</sup>C NMR.

To test the reusability of the catalyst, the single used CuO nanostructures (sample CuO-2) were first washed with water followed by ethanol to remove any other surface-adsorbed organic components. The dispersed solid catalyst was then isolated by centrifugation and repeated washing with a water–ethanol mixture. The solid catalyst was dried overnight in a vacuum oven at 60 °C and was reused in new batches of the aza-Michael reaction.

# 3. Results and discussion

## 3.1 X-Ray diffraction studies

The X-Ray powder diffraction technique was used to check the purity and to determine the phase structure of the as-prepared samples. The sharp and intense diffraction peaks in all the samples shown in Fig. 1 match completely with the XRD pattern of monoclinic phase CuO (JCPDS file No.: 48-1548; stick pattern) indicating the formation of highly crystalline CuO nanostructures. The diffraction peaks that appeared at  $2\theta = 32.7, 35.7, 39.0, 49.0, 53.7, 58.5, 61.8, 66.3, 68.3, 72.8$  and  $75.4^\circ$  are assigned to the planes (110), (002)/( $\bar{1}11$ ), (111)/(200), ( $\bar{2}02$ ), (020), (202), ( $\bar{1}13$ ), (113), (220), (311) and (004), respectively.<sup>10,29</sup> The absence of other diffraction peaks due to any impurities indicated the formation of pure and well-crystallized CuO nanostructures.

## 3.2 Electron microscopy analysis

To gain insight into the surface topography of the as-synthesized CuO nanostructures, SEM analysis was carried out on all the



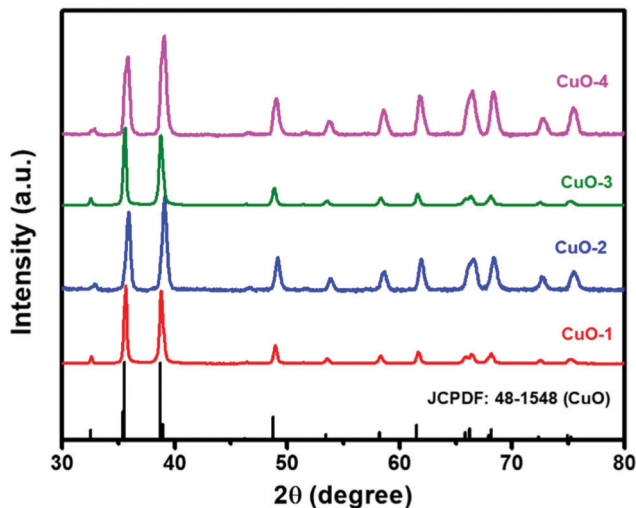


Fig. 1 XRD patterns of different samples of CuO nanostructures as compared with the reference pattern of tenorite, CuO.

samples (Fig. 2). Fig. 2a shows the SEM image of sample CuO-1 prepared in the presence of 1.0 wt% seed shell extract of *Sapindus mukorossi*. The micrograph clearly shows the formation of globular shaped particles of sizes varying from 67 to 135 nm. Furthermore, it is also clear from the micrograph that two–three of such globular particles are assembled either linearly or sideways to form short rod or branched structures. Almost no isolated particles were noticed in the micrograph. To investigate the effect of the extract concentration, another sample (CuO-2) was prepared in the presence of 0.5 wt% extract, keeping all other reaction conditions the same. The SEM image of this sample (Fig. 2b) shows the formation of particles quite similar to those observed in sample CuO-1. However, the sizes of these particles in sample CuO-2 ranges

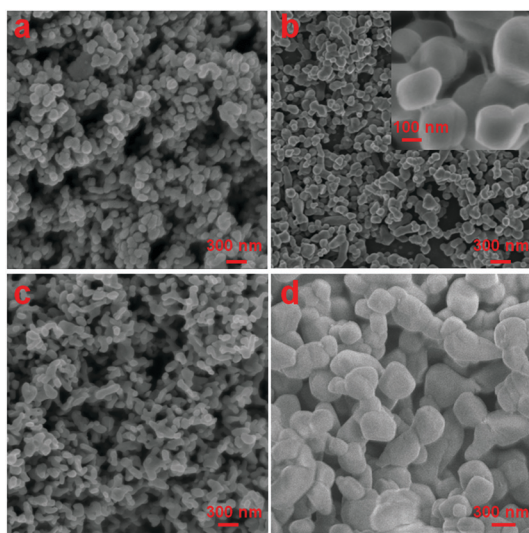


Fig. 2 SEM images of the synthesized CuO nanostructures: samples (a) CuO-1, (b) CuO-2, (c) CuO-3 and (d) CuO-4. The inset in (b) shows the magnified image of sample CuO-2.

from 76 to 140 nm. To check the exact surface topography, a magnified portion of Fig. 2b was recorded (inset in Fig. 2b), which clearly shows that the individual particles are not purely globular but rather they have some undefined geometrical shape, the surface of which is flattened. A further decrease in the extract concentration to 0.25 wt% (sample CuO-3) resulted again in the formation of similar elongated and branched structures (Fig. 2c). The sizes of the globular particles, which are assumed to be assembled to produce these elongated and branched structures, vary from 80 to 145 nm. Furthermore, to ascertain the effect of the plant extract on the morphology and size of the CuO nanostructures, another sample was synthesized in the absence of the extract (sample CuO-4). The SEM image recorded from this sample (Fig. 2d) again shows the presence of a similar morphology, but the sizes of these particles are larger (215 to 430 nm) than those of the previous samples prepared in the presence of the *Sapindus mukorossi* seed shell extract. These results indicate that the plant extract plays a crucial role in controlling the size of the CuO nanostructures, but it does not have any impact on the morphology of the formed nanostructures. Moreover, as the concentration of the plant extract is increased, the sizes of the formed nanostructures decrease. This is attributed to the capping efficiency of the phytochemicals present in the extract towards the growing nuclei during their formation. Furthermore, to ascertain the composition of the product, the energy dispersive X-ray (EDX) spectrum and elemental mapping were recorded from sample CuO-2 (Fig. 3). The EDX spectrum shown in Fig. 3a shows the peaks due to elemental Cu and O with an atomic ratio of 1 : 1.05, confirming that the product is CuO. The peaks due to C (the low-energy region) and Pt are assigned to the carbon tape used to hold the sample and sputtering coating of the materials. Fig. 3c and d show the mapping results of Cu and O, respectively, supporting the EDX results.

To confirm the morphological evolution further, the TEM images of samples CuO-2, CuO-3 and CuO-4 were recorded (Fig. 4). The micrographs of all the samples (Fig. 4a–c) clearly

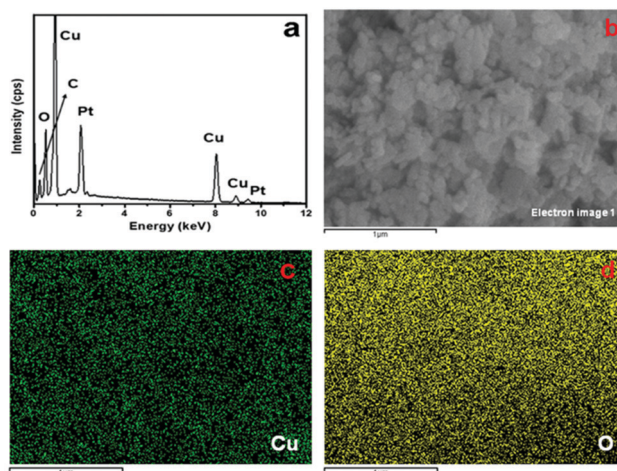


Fig. 3 (a) EDX spectrum, (b) SEM electron image, and elemental mapping of (c) Cu and (d) O of CuO nanostructures (sample CuO-2).



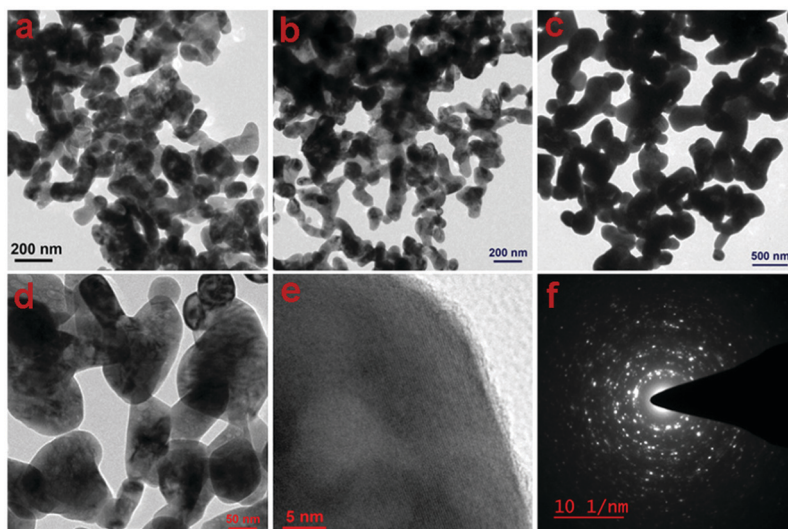


Fig. 4 TEM images of CuO nanostructures recorded from samples (a) CuO-2, (b) CuO-3, and (c) CuO-4. (d) Magnified TEM image of sample CuO-2, (e) HRTEM image recorded from a portion of a particle in sample CuO-2, and (f) the corresponding SAED pattern.

show the presence of CuO nanostructures, which seem to be formed by the fusion of two–three individual CuO nanoparticles during the calcination process. In addition, the presence of some voids (light spots) could be noticed within the particles as confirmed from the high-magnification TEM image (Fig. 4d) recorded from a portion of sample CuO-2. Furthermore, to gain insight into the inner structure, a high-resolution TEM (HRTEM) image from sample CuO-2 was recorded (Fig. 4e), which shows the presence of perfectly aligned lattice fringes. The interplane space ( $d$  spacing) value as calculated from this micrograph is 0.275 nm, which corresponds to the (110) plane of CuO.<sup>29</sup> The SAED patterns recorded from these samples are similar and so only a representative SAED pattern of sample CuO-2 is presented in Fig. 4f. The presence of bright spots superimposed on ring patterns confirms the polycrystalline nature of the particles with possible defects on their surfaces.

### 3.3 FTIR spectroscopy study

To investigate the surface functionalities, FTIR spectra were recorded from the seed shell extract of *Sapindus mukorossi*, from sample CuO-2 prepared in the presence of 0.5 wt% of the seed shell extract, and from sample CuO-4 prepared in the absence of the extract (Fig. 5). The spectrum of seed shell extract exhibited absorption peaks at 3420, 2938, 2852 (weak), 1739, 1251, and 1046  $\text{cm}^{-1}$ . The broad peak at 3420  $\text{cm}^{-1}$  is assigned to the alcoholic O–H stretching from flavonols present in the plant extract, which is further confirmed by the presence of an intense peak at 1046  $\text{cm}^{-1}$  due to the C–O stretching vibration in alcohols.<sup>61</sup> The strong band at 2938  $\text{cm}^{-1}$  corresponds to the aliphatic C–H asymmetric stretching vibration, while the low-intensity absorption peak at 2852  $\text{cm}^{-1}$  is assigned to the C–H stretching vibration.<sup>62</sup> The peaks at 1739 and 1251  $\text{cm}^{-1}$  are characteristic of the C=O stretching and C–O bending vibrations, respectively.<sup>61</sup> The peak at 657  $\text{cm}^{-1}$  is due to the presence of the alkyne group in the biomolecules.

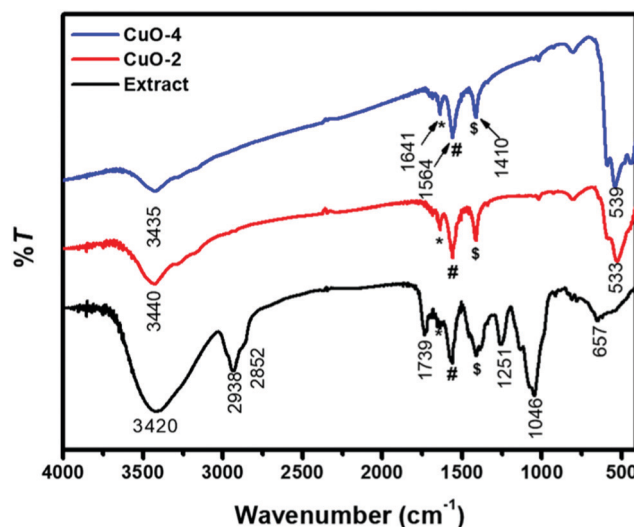


Fig. 5 FTIR spectra of the seed shell extract of the *Sapindus mukorossi* plant and CuO nanostructures. Samples CuO-2 and CuO-4 are prepared in the presence and absence of the extract, respectively.

The FTIR spectra of samples CuO-2 and CuO-4 exhibited a broad peak in the range of 3535–3400  $\text{cm}^{-1}$ , which is due to O–H stretching from surface-adsorbed water molecules. The peaks that appear in the FTIR spectra of samples CuO-2 and CuO-4 in the region of 530–536  $\text{cm}^{-1}$  are due to the Cu–O stretching vibration of CuO.<sup>62</sup> The peaks observed in all the samples including the plant extract at around 1641, 1564, and 1410  $\text{cm}^{-1}$  (marked by \*, # and \$, respectively) are due to free carbonate, and the asymmetric and symmetric O–C–O stretching vibration of the adsorbed carbonate anion, respectively.<sup>63</sup> It is evident from the FTIR spectroscopy study that the plant molecules are burned away during calcination and so no functional groups on the surface of CuO synthesized in the presence of the plant extract could be detected.



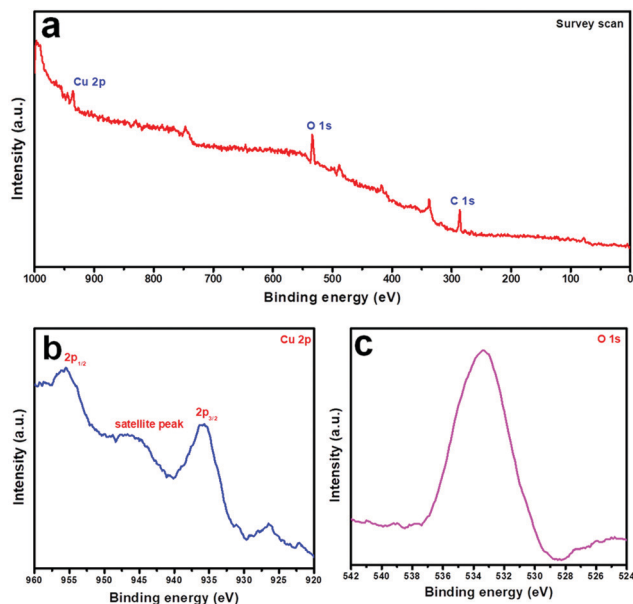


Fig. 6 X-Ray photoelectron spectra of CuO nanostructures (sample CuO-2): (a) survey scan, (b) Cu 2p, and (c) O 1s region.

### 3.4 N<sub>2</sub> gas adsorption–desorption study

To study the effect of the plant extract on the surface properties of the CuO nanostructures, a N<sub>2</sub> gas adsorption–desorption study was carried out on samples CuO-2 and CuO-4, prepared in the presence and the absence of the plant extract, respectively. The N<sub>2</sub> gas adsorption–desorption curves of both samples CuO-2 and CuO-4, as shown in Fig. S1 in the ESI,<sup>†</sup> displayed a type H3 hysteresis loop, which is characteristic of slit-shaped pores formed by the aggregation of plate-like particles.<sup>64</sup> Furthermore, they follow a type II isotherm, which is characteristic of mesoporous materials.<sup>64</sup> The Brunauer–Emmett–Teller (BET) surface area, as measured from the multi-point curve, was found to be 9.9 and 4.8 m<sup>2</sup> g<sup>-1</sup> for samples CuO-2 and CuO-4, respectively. The enhanced surface area of sample CuO-2 prepared in the presence of the seed shell extract is attributed to the smaller size and different surface characteristics compared with sample CuO-4. The observed BET surface area is higher than that reported for CuO NPs prepared using similar methods.<sup>58</sup> Furthermore, sample CuO-2 also possesses a higher pore volume of 0.018 cm<sup>3</sup> g<sup>-1</sup>, against 0.008 cm<sup>3</sup> g<sup>-1</sup> of CuO-4. However, sample CuO-4 exhibited a higher pore diameter (2.465 nm) compared with sample CuO-2 (2.184 nm). This might be attributed to a larger gap in between the particles due to their larger size. The results further indicated the formation of mesoporous materials during calcination.

### 3.5 X-Ray photoelectron spectroscopy analysis

To understand the elemental composition and the oxidation state of the individual elements in the products, an X-ray photoelectron spectroscopy (XPS) study was performed on sample CuO-2. The survey scan spectrum (Fig. 6a) shows the presence of elemental peaks due to Cu 2p, and O 1s. Fig. 6b depicts

Table 2 Optimization of aza-Michael reaction conditions using the as-synthesized CuO nanostructures (sample CuO-2) as the catalyst<sup>a</sup>

Entry	Amount of catalyst (mg)	Solvent	Temperature (°C)	Time (h)	Yield <sup>b</sup> (%)
1	—	Solvent-free	r.t.	20	30
2	—	Solvent-free	45	12	40
3	7	Solvent-free	45	9	50
4	7	Water	45	6	60
5	7	Diethylene glycol	45	12	Trace
6	7	<i>N,N</i> -Dimethylformamide (DMF)	45	12	30
7	7	DMF + water (V/V = 1 : 1)	45	12	50
8	7	Methanol	45	12	50
9	7	Methanol + water (V/V = 1 : 1)	45	12	60
10	7	Isopropanol	45	12	Trace
11	7	Isopropanol + water (V/V = 1 : 1)	45	9	50
12	7	Acetonitrile	45	12	Trace
13	7	Ethanol	45	6	40
14	7	Ethanol + water (V/V = 1 : 1)	45	6	80
15	5	Ethanol + water (V/V = 1 : 1)	45	6	80
16	2	Ethanol + water (V/V = 1 : 1)	45	6	80
17	1	Ethanol + water (V/V = 1 : 1)	45	6	50
18	2	Ethanol + water (V/V = 1 : 1)	rt	6	58
19	2	Ethanol + water (V/V = 1 : 1)	60	6	77

<sup>a</sup> Reaction conditions: aniline (1.0 mmol), and acrylonitrile (2.5 mmol).

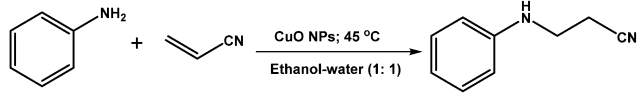
<sup>b</sup> Isolated yield.

the high-resolution XPS spectrum of the Cu 2p region, which shows intense peaks at binding energies 935.8 and 955.6 eV due to Cu 2p<sub>3/2</sub> and Cu 2p<sub>1/2</sub>, respectively. The energy gap of 19.8 eV between the Cu 2p<sub>3/2</sub> and Cu 2p<sub>1/2</sub> peaks is very close to the standard value of Cu 2p in CuO.<sup>29</sup> Besides, a broad shake-up satellite due to Cu<sup>2+</sup> was observed at 946.1 eV. These results confirm the presence of Cu in the +2 oxidation state in the products, ruling out the possibility of the presence of the Cu<sub>2</sub>O phase. Fig. 6c shows the O 1s core-level spectrum, where a sharp peak at 533.4 eV can be observed due to O<sup>2-</sup> in the CuO crystal lattice. The results confirmed that the composition of the sample is CuO.

### 3.6 Catalytic activity study

To check the catalytic efficiency of the synthesized CuO nanostructures, the aza-Michael reaction was chosen as a model reaction. To optimize the reaction conditions, at the outset, the reaction of aniline (1.0 mmol) and acrylonitrile (2.5 mmol) was chosen as the substrate at room temperature without any solvent and catalyst, but the reaction resulted in a very low yield (approximately 30%) of the product even after 20 h (Table 2; entry 1). In a new set of similar reactions when the temperature was increased to 45 °C the yield of the product was improved in 12 h (Table 2; entry 2). When a small amount of the CuO nanostructures (7.0 mg; sample CuO-2) was added to the reaction mixture, we were surprised to see an improvement in the yield of the product within 9 h (Table 2; entry 3). Then, we



**Table 3** Effect of catalyst and catalyst loading in the aza-Michael reaction<sup>a</sup>


Entry	Catalyst	Time (h)	Yield <sup>b</sup> (%)
1	CuO-1	6	80
2	CuO-2	6	80
3	CuO-3	6	80
4	CuO-4	6	60
5	<sup>c</sup> CuO-2	6	60

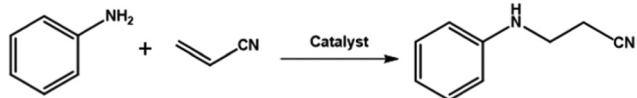
<sup>a</sup> Reaction conditions: aniline (1.0 mmol), acrylonitrile (2.5 mmol); catalyst (2.0 mg). <sup>b</sup> Isolated yield. <sup>c</sup> Before calcination.

tested the reaction using different solvent systems at 45 °C (Table 2; entries 4–14) and observed that when the solvent system is a mixture of water (0.5 mL) and ethanol (0.5 mL) in the volume ratio of 1 : 1, the highest yield of 80% of the product was obtained after 6 h (Table 2; entry 14). This might be due to the enhanced solubility of the reactants in a solvent of suitable polarity, which can be adjusted by changing the water : ethanol ratio in the aza-Michael reaction. In the next assessment, the performance of the catalyst was tested with different catalyst loadings (Table 2; entries 15–17). It was observed that 7.0, 5.0 and 2.0 mg of the catalyst (sample CuO-2) were equally efficient in the current reaction (Table 2; entries 14–16). However, the performance of the catalyst was significantly decreased when the catalyst loading was lowered to 1.0 mg (Table 2; entry 17). Hence, in the current study, the catalyst loading was fixed at 2 mg for the remaining experiments. Furthermore, to find the optimum temperature with the catalyst loading of 2 mg, the reaction was performed at room temperature and 60 °C (Table 2; entries 18 and 19). It was observed that when the reaction was carried out at room temperature the yield was decreased to 58%, whereas at 60 °C the yield was 77%, which is very close to the yield at 45 °C. So, the optimum temperature for the reaction system was considered to be 45 °C.

To test the catalytic activity of the other synthesized CuO nanostructures we repeated the reaction between aniline and

acrylonitrile in the solvent mixture of water (0.5 mL) and ethanol (0.5 mL) (V/V = 1 : 1) at 45 °C, fixing the catalyst amount at 2.0 mg and keeping other reaction parameters fixed. It is evident from Table 3 that all the catalysts prepared in the presence of the plant extract offer a higher catalytic activity compared with those prepared in the absence of the plant extract. We also tested the catalytic activity of sample CuO-2 without calcination, which offered 60% yield in 6 h. Moreover, the CuO nanostructures synthesized without using any capping agent (sample CuO-4) could produce a 60% yield in 6 h under the same reaction conditions. The probable reason behind the enhanced catalytic activity of CuO nanostructures prepared in the presence of the seed shell extract of *Sapindus mukorossi* might be due to their increased surface area because of their smaller size and surface properties, as confirmed from BET surface area analysis. Furthermore, to examine the effectiveness of the current protocol, the results of the current study are compared with other heterogeneous catalyst systems (Table 4). The comparative study revealed the effectiveness of the current catalyst system in the aza-Michael reaction between aniline and acrylonitrile. It is also noticed that most of the catalysts required either support materials, which played a major role in the enhanced activity of the catalyst, or acidic or alkaline media. By contrast, the current catalyst needs neither a support nor the presence of acid, base or ligand in the medium.

With the optimized reaction conditions in hand, we expanded the aza-Michael reaction using some substituted anilines and other amines. It was observed that the substituted anilines having electron-donating alkyl groups at the *ortho*, *para* and *meta* positions were found to be good reactants towards the aza-Michael reaction under the proposed protocol (Table 5 entries 2–5). However, the electron-deficient anilines are unable to yield respective products under the proposed conditions (Table 5 entries 6 and 7). This might be due to the high deficiency of non-bonding electron pairs on the nitrogen of the amine group to undergo the aza-Michael reaction with acrylonitrile. Also, a low yield of the product was observed with a primary aliphatic amine (Table 5 entry 8), which might be due to the fact that the reaction was performed under mild reaction conditions. It has been reported that such amines are effective

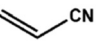
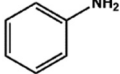
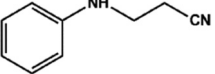
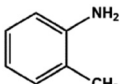
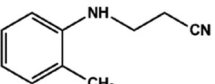
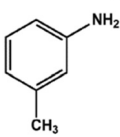
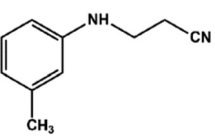
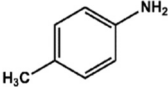
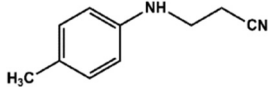
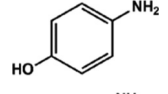
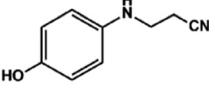
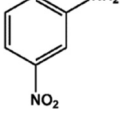
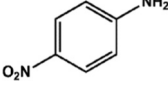
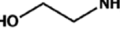
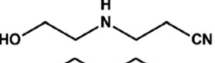
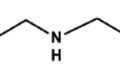
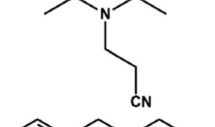
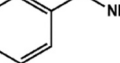
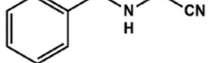
**Table 4** Comparison of the efficiency of the current catalyst in the aza-Michael reaction


Entry	Catalyst	Amount	Solvent/temperature/time	Yield (%)
1	Starch-supported organocatalyst (ES-SO <sub>3</sub> <sup>-</sup> -C <sub>5</sub> H <sub>5</sub> NH <sup>+</sup> ) <sup>54</sup>	1 mol%	THF/r.t./3 h	65
2	SiO <sub>2</sub> -supported AlCl <sub>3</sub> <sup>52</sup>	200 mg	Solventless/60 °C/6 h	75
3	Graphene oxide <sup>53</sup>	0.5 ml suspension	Water/r.t./45 min	65
4	Ionic liquid-based [TMPSA][HSO <sub>4</sub> ] <sup>65</sup>	1 mmol	Water/r.t./4 h	87
5	Acidic alumina <sup>66</sup>	200 mg	Solventless/r.t./3 h	90 <sup>a</sup>
6	Phen-MCM-Br <sub>2</sub> <sup>55</sup>	70 mg	Water/r.t./2.5 h	80
7	Nano CuO (this work)	2 mg	Ethanol-water mixture/45 °C/6 h	80

<sup>a</sup> The reaction was performed under acidic conditions.



Table 5 Substrate scope for the aza-Michael reaction under thermal conditions<sup>a</sup>

Amine + 		CuO NPs; 45 °C Ethanol-water (1: 1)		Product	
Entry	Amine	Product	Time (h)	Yield <sup>b</sup> (%)	
1			6	80	
2			6	85	
3			6	90	
4			6	90	
5			6	87	
6		No product	6	x	
7		No product	6	x	
8			5	60	
9			1	85	
10			6	80	

<sup>a</sup> Reaction conditions: amine (1.0 mmol), acrylonitrile (2.5 mmol); catalyst (2.0 mg). <sup>b</sup> Isolated yield.

only under harsh reaction conditions, and that is why we observed such a low conversion.<sup>29,67</sup> The developed protocol was also found to be efficient for other primary and secondary amines (Table 5 entries 9 and 10).

### 3.7 Reusability of CuO nanostructures as the catalyst

To test the reusability of the catalyst, the used CuO nanostructures (sample CuO-2) were isolated and purified to get rid of any surface-adsorbed organic components, as discussed in Section 2.4. The isolated dried solid catalyst was reused in new batches of the aza-Michael reaction. Fig. 7 shows that the CuO nanostructures could be reused up to a 5th cycle without any significant loss in catalytic activity, after which the catalytic

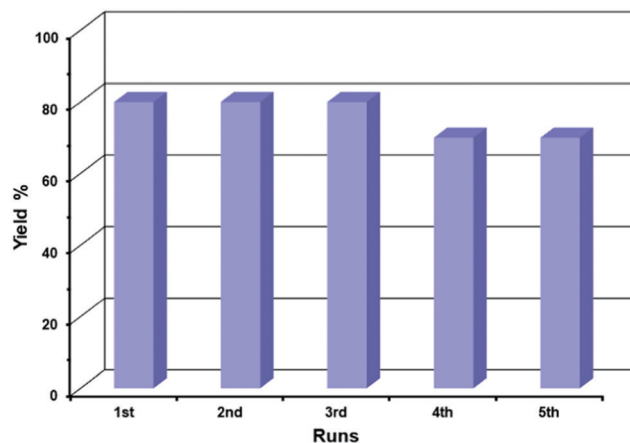


Fig. 7 Bar diagram showing recycling data of the catalytic activity.

activity decreased gradually. The reason for the decreasing catalytic activity of the CuO nanostructures might be due to the adsorption of some organic components on the surface of the CuO or the conversion of some CuO nanostructures into Cu<sub>2</sub>O either during catalysis or washing. This was confirmed from the XRD pattern of reused CuO nanostructures where additional diffraction peaks at  $2\theta = 36.5$  and  $42.4^\circ$ , which correspond to the (111) and (200) crystalline planes of the cubic phase of Cu<sub>2</sub>O, could be observed (Fig. 8a).<sup>68</sup> However, the structure of the catalyst remains intact during the catalysis (Fig. 8b). It has been reported that Cu NPs can be used in the aza-Michael reaction conveniently under mild reaction conditions.<sup>7</sup> However, it was found that Cu NPs are more toxic than CuO NPs, which makes CuO NPs a better candidate for catalysis reactions.<sup>69</sup> In addition, CuO NP-catalyzed aza-Michael reactions have several advantages, but most of the reported methods suffer from some specific drawbacks in the large-scale production of CuO NPs in industry, such as the use of toxic solvents,<sup>57</sup> and the use of high-energy and long-time exposure of ultrasonic waves.<sup>29</sup> By contrast, the proposed protocol for the aza-Michael reaction requires a green solvent system (*i.e.*, a mixture of ethanol and water) and low-temperature conditions (45 °C). Moreover, the CuO nanocatalysts used in this study are synthesized without using any toxic capping

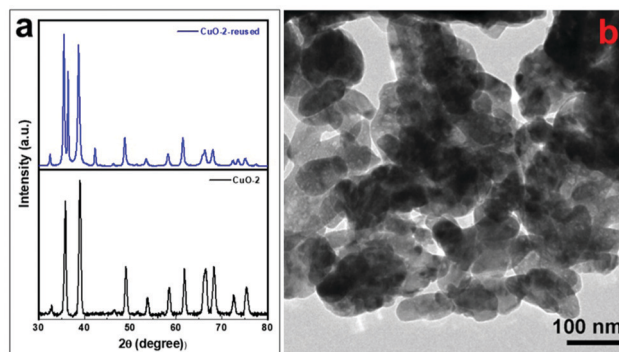


Fig. 8 (a) XRD pattern of sample CuO-2 before and after catalysis and (b) TEM image of sample CuO-2 after catalysis.





agent; instead, the seed shell extract of the *Sapindus mukorossi* plant is used.

## 4. Conclusion

CuO nanostructures have been synthesized using a hydrothermal method in the presence of the seed shell extract of the *Sapindus mukorossi* plant followed by calcination of the product at 500 °C for 4 h in air. The phytochemicals present in the seed shell extract play the role of stabilizer and capping agent, as confirmed by control experiments. The XRD study confirmed the formation of highly crystalline CuO nanostructures in the monoclinic phase which are free from any impurities. The as-synthesized CuO NPs exhibit excellent catalytic activity towards the aza-Michael reaction of acrylonitrile with primary and secondary aliphatic and aromatic amines at 45 °C in a mixed solvent system of ethanol and water in the volume ratio of 1 : 1. Also, the proposed catalyst is more effective than other supported catalysts that need the presence of an acid, base or ligand. CuO, being a non-toxic material, provides a greener pathway for a variety of substituted aza-Michael products with moderate to excellent yields. Also, the catalysts are reusable up to the 5th catalytic cycle without any significant loss of catalytic activity.

## Author contributions

Tulan Chandra Saikia: conceptualization, methodology, formal analysis and investigation, and original draft preparation. Saddam Iraqui: formal analysis and investigation. Aslam Khan: resources, formal analysis. Md. Harunar Rashid: supervision, conceptualization, and reviewing and editing.

## Conflicts of interest

The authors declare no conflict of interest.

## Acknowledgements

MHR acknowledges the Council of Scientific and Industrial Research, India (Grant No. 01(2910)/17/EMR-II) for partially supporting the research. The authors also thank SAIF, NEHU, NEIST, Jorhat, CIF-GU, SAIC, TU, and MARC, Bangalore for extending instrumental facilities to us.

## References

- 1 M. Kamalgharibi, F. Hormozi, S. A. H. Zamzamin and M. M. Sarafraz, *Heat Mass Trans.*, 2016, **52**, 55–62.
- 2 M. Liu, M. C. Lin and C. Wang, *Nanoscale Res. Lett.*, 2011, **6**, 297.
- 3 S. Meghana, P. Kabra, S. Chakraborty and N. Padmavathy, *RSC Adv.*, 2015, **5**, 12293–12299.
- 4 J. Sackey, A. C. Nwanya, A. K. H. Bashir, N. Matinise, J. B. Ngilirabanga, A. E. Ameh, E. Coetsee and M. Maaza, *Mater. Chem. Phys.*, 2020, **244**, 122714.
- 5 H. Siddiqui, M. R. Parra, P. Pandey, M. S. Qureshi and F. Z. Haque, *J. Sci.: Adv. Mater. Dev.*, 2020, **5**, 104–110.
- 6 B. Ameri, S. S. H. Davarani, R. Roshani, H. R. Moazami and A. Tadjarodi, *J. Alloys Compd.*, 2017, **695**, 114–123.
- 7 M. B. Gawande, A. Goswami, F.-X. Felpin, T. Asefa, X. Huang, R. Silva, X. Zou, R. Zboril and R. S. Varma, *Chem. Rev.*, 2016, **116**, 3722–3811.
- 8 S. Jammi, S. Sakthivel, L. Rout, T. Mukherjee, S. Mandal, R. Mitra, P. Saha and T. Punniyamurthy, *J. Org. Chem.*, 2009, **74**, 1971–1976.
- 9 M. Nasrollahzadeh, S. M. Sajadi, A. Rostami-Vartooni and S. M. Hussin, *J. Colloid Interface Sci.*, 2016, **466**, 113–119.
- 10 J. K. Sharma, M. S. Akhtar, S. Ameen, P. Srivastava and G. Singh, *J. Alloys Compd.*, 2015, **632**, 321–325.
- 11 P. K. Singh, A. K. Das, G. Hatui and G. C. Nayak, *Mater. Chem. Phys.*, 2017, **198**, 16–34.
- 12 V. Singh and P. Bansal, *Mater. Lett.*, 2020, **261**, 126929.
- 13 N. Verma and N. Kumar, *ACS Biomater. Sci. Eng.*, 2019, **5**, 1170–1188.
- 14 F. Wang, H. Li, Z. Yuan, Y. Sun, F. Chang, H. Deng, L. Xie and H. Li, *RSC Adv.*, 2016, **6**, 79343–79349.
- 15 R. Poreddy, C. Engelbrekt and A. Riisager, *Catal. Sci. Technol.*, 2015, **5**, 2467–2477.
- 16 L. Rout, T. K. Sen and T. Punniyamurthy, *Angew. Chem., Int. Ed.*, 2007, **46**, 5583–5586.
- 17 D. Astruc, *Chem. Rev.*, 2020, **120**, 461–463.
- 18 S. Cao, F. Tao, Y. Tang, Y. Li and J. Yu, *Chem. Soc. Rev.*, 2016, **45**, 4747–4765.
- 19 Z. Li, J. Wang, N. Wang, S. Yan, W. Liu, Y. Q. Fu and Z. Wang, *J. Alloys Compd.*, 2017, **725**, 1136–1143.
- 20 A. E. Nogueira, A. S. Giroto, A. B. S. Neto and C. Ribeiro, *Colloids Surf., A*, 2016, **498**, 161–167.
- 21 H. N. Cuong, S. Pansambal, S. Ghotekar, R. Oza, N. T. Thanh Hai, N. M. Viet and V.-H. Nguyen, *Environ. Res.*, 2022, **203**, 111858.
- 22 A. M. E. Shafey, *Green Process. Synth.*, 2020, **9**, 304–339.
- 23 A. Waris, M. Din, A. Ali, M. Ali, S. Afridi, A. Baset and A. Ullah Khan, *Inorg. Chem. Commun.*, 2021, **123**, 108369.
- 24 F. A. Bezza, S. M. Tichapondwa and E. M. N. Chirwa, *Sci. Rep.*, 2020, **10**, 16680.
- 25 M. Taran, M. Rad and M. Alavi, *Pharm. Sci.*, 2017, **23**, 198–206.
- 26 M. Hariram and S. Vivekanandhan, *ChemistrySelect*, 2018, **3**, 13561–13585.
- 27 N. Nagar and V. Devra, *Mater. Chem. Phys.*, 2018, **213**, 44–51.
- 28 R. Sankar, P. Manikandan, V. Malarvizhi, T. Fathima, K. S. Shivashangari and V. Ravikumar, *Spectrochim. Acta, Part A*, 2014, **121**, 746–750.
- 29 R. Chowdhury, A. Khan and M. H. Rashid, *RSC Adv.*, 2020, **10**, 14374–14385.
- 30 S. Suresh, R. Ilakiya, G. Kalaiyan, S. Thambidurai, P. Kannan, K. M. Prabu, N. Suresh, R. Jothilakshmi, S. Karthick Kumar and M. Kandasamy, *Ceram. Int.*, 2020, **46**, 12525–12537.



- 31 K. Anitha, Y. Jyothi, V. Veena and D. Bora, *J. Chem. Pharm. Res.*, 2015, **7**, 363–368.
- 32 S. Goyal, *J. Drug Delivery Ther.*, 2014, **4**, 7–20.
- 33 R. Singh and B. Sharma, *Biotechnological advances, phytochemical analysis and ethnomedical implications of sapindus species*, Springer, Singapore, 1 edn, 2019.
- 34 N. Yekeen, A. A. Malik, A. K. Idris, N. I. Reepei and K. Ganie, *J. Petrol. Sci. Eng.*, 2020, **195**, 107591.
- 35 V. N. M. Devi, M. Rajakohila, L. A. M. Syndia, P. N. Prasad and V. N. Ariharan, *Res. J. Pharm. Biol. Chem. Sci.*, 2012, **3**, 420–424.
- 36 I. Azhar, *Pak. J. Pharm. Sci.*, 1994, **7**, 33–41.
- 37 R. K. Borah, A. Mahanta, A. Dutta, U. Bora and A. J. Thakur, *Appl. Organometal. Chem.*, 2017, **31**, e3784.
- 38 G. Dinda, D. Halder, A. Mitra, N. Pal, C. Vázquez-Vázquez and M. A. López-Quintela, *New J. Chem.*, 2017, **41**, 10703–10711.
- 39 V. Reddy, R. S. Torati, S. Oh and C. Kim, *Ind. Eng. Chem. Res.*, 2013, **52**, 556–564.
- 40 V. Jassal, U. Shanker, S. Gahlot, B. S. Kaith, Kamaluddin, M. A. Iqubal and P. Samuel, *Appl. Phys. A: Mater. Sci. Process.*, 2016, **122**, 271.
- 41 M. Liu and M. P. Sibi, *Tetrahedron*, 2002, **58**, 7991–8035.
- 42 M. G. Vinogradov, O. V. Turova and S. G. Zlotin, *Org. Biomol. Chem.*, 2019, **17**, 3670–3708.
- 43 S. Azad, T. Kobayashi, K. Nakano, Y. Ichikawa and H. Kotsuki, *Tetrahedron Lett.*, 2009, **50**, 48–50.
- 44 M. K. Chaudhuri, S. Hussain, M. L. Kantam and B. Neelima, *Tetrahedron Lett.*, 2005, **46**, 8329–8331.
- 45 N. Azizi and M. R. Saidi, *Tetrahedron*, 2004, **60**, 383–387.
- 46 L. Fadini and A. Togni, *Chem. Commun.*, 2003, 30–31, DOI: 10.1039/b210680a.
- 47 N. Srivastava and B. K. Banik, *J. Org. Chem.*, 2003, **68**, 2109–2114.
- 48 S. Kobayashi, K. Kakumoto and M. Sugiura, *Org. Lett.*, 2002, **4**, 1319–1322.
- 49 L.-W. Xu, C.-G. Xia and X.-X. Hu, *Chem. Commun.*, 2003, 2570–2571, DOI: 10.1039/b307733k.
- 50 S. Albonetti, R. Mazzoni and F. Cavani, in *Transition Metal Catalysis in Aerobic Alcohol Oxidation*, ed. F. Cardona and C. Parmeggiani, The Royal Society of Chemistry, 2015, DOI: 10.1039/9781782621652-00001, ch. 1, pp. 1–39.
- 51 N. Mizuno and M. Misono, *Chem. Rev.*, 1998, **98**, 199–218.
- 52 M. R. Saidi, Y. Pourshojaei and F. Aryanassab, *Synth. Commun.*, 2009, **39**, 1109–1119.
- 53 S. Verma, H. P. Mungse, N. Kumar, S. Choudhary, S. L. Jain, B. Sain and O. P. Khatri, *Chem. Commun.*, 2011, **47**, 12673–12675.
- 54 S. Verma, S. L. Jain and B. Sain, *Org. Biomol. Chem.*, 2011, **9**, 2314–2318.
- 55 R. Hosseinzadeh, N. Aghili and M. Tajbakhsh, *Catal. Lett.*, 2016, **146**, 1194–1203.
- 56 N. S. Shaikh, V. H. Deshpande and A. V. Bedekar, *Tetrahedron*, 2001, **57**, 9045–9048.
- 57 M. L. Kantam, S. Laha, J. Yadav and S. Jha, *Tetrahedron Lett.*, 2009, **50**, 4467–4469.
- 58 A. F. Zedan, A. T. Mohamed, M. S. El-Shall, S. Y. AlQaradawi and A. S. AlJaber, *RSC Adv.*, 2018, **8**, 19499–19511.
- 59 D. Zhan, T. Li, H. Wei, W. Weng, K. Ghandi and Q. Zeng, *RSC Adv.*, 2013, **3**, 9325–9329.
- 60 S. Konar, H. Kalita, N. Puvvada, S. Tantubay, M. K. Mahto, S. Biswas and A. Pathak, *J. Catal.*, 2016, **336**, 11–22.
- 61 V. T. L. Huong and N. T. Nguyen, *Mater. Today: Proc.*, 2021, **42**, 88–93.
- 62 A. Bhattacharjee and M. Ahmaruzzaman, *RSC Adv.*, 2016, **6**, 41348–41363.
- 63 K. Coenen, F. Gallucci, B. Mezari, E. Hensen and M. van Sint Annaland, *J. CO<sub>2</sub> Util.*, 2018, **24**, 228–239.
- 64 K. S. W. Sing, D. H. Everett, R. A. W. Haul, L. Moscou, R. A. Pierotti, J. Rouquerol and T. Siemieniowska, *Pure Appl. Chem.*, 1985, **57**, 603–619.
- 65 X. Liu, M. Lu, G. Gu and T. Lu, *J. Iran. Chem. Soc.*, 2011, **8**, 775–781.
- 66 G. Bosica and R. Abdilla, *Molecules*, 2016, **21**, 815.
- 67 A. K. Verma, R. Kumar, P. Chaudhary, A. Saxena, R. Shankar, S. Mozumdar and R. Chandra, *Tetrahedron Lett.*, 2005, **46**, 5229–5232.
- 68 A. Sahai, N. Goswami, S. D. Kaushik and S. Tripathi, *Appl. Surf. Sci.*, 2016, **390**, 974–983.
- 69 F. Wu, B. J. Harper, L. E. Crandon and S. L. Harper, *Environ. Sci.: Nano*, 2020, **7**, 105–115.

